Modern Physics Letters A
© World Scientific Publishing Company

arXiv:1405.7217v1 [hep-ex] 28 May 2014

Reactor Neutrino Experiments: θ_{13} and Beyond

Xin Qian*
Brookhaven National Laboratory,
Upton, NY, 11973, USA

Wei Wang†
Physics Department, College of William and Mary
Williamsburg, VA, 23187, USA

Received (Day Month Year)
Revised (Day Month Year)

We review the current-generation short-baseline reactor neutrino experiments that have firmly established the third neutrino mixing angle θ_{13} to be non-zero. The relative large value of θ_{13} (around 9°) has opened many new and exciting opportunities for future neutrino experiments. Daya Bay experiment with the first measurement of Δm^2_{ee} is aiming for a precision measurement of this atmospheric mass-squared splitting with a comparable precision as $\Delta m^2_{\mu\mu}$ from accelerator muon neutrino experiments. JUNO, a next-generation reactor neutrino experiment, is targeting to determine the neutrino mass hierarchy with medium baselines (∼50 km). Beside these opportunities enabled by the large θ_{13}, the current-generation (Daya Bay, Double Chooz, and RENO) and the next-generation (JUNO, RENO-50, and PROSPECT) reactor experiments, with their unprecedented statistics, are also leading the precision era of the 3-flavor neutrino oscillation physics as well as constraining new physics beyond the neutrino Standard Model.

Keywords: θ_{13}, precision measurements, mass hierarchy

PACS Nos.: include PACS Nos.

1. Introduction

Reactor neutrinos have been playing a crucial role in the development of the Standard Model and the 3-flavor neutrino framework. In 1956, Cowan and Reines discovered neutrinos at the Savannah River reactor power plant in the U.S. [1]. In 2005, KamLAND experiment in Japan observed the neutrino oscillation in the solar sector [2]. Their finding together with those from SNO experiment [3] in Canada firmly established the neutrino oscillation as the explanation of the solar neutrino puzzle. [a]

*email:xqian@bnl.gov
†email:wswang@wm.edu
[a]The solar neutrino puzzle refers to a major discrepancy between measurements of the number of ν_e going through earth and that predicted by the standard solar model.

Most recently, Daya Bay experiment in China reported the discovery of non-zero θ_{13}, the third neutrino mixing angle, with a significance $>5\sigma$ in 2012 [4]. The non-zero θ_{13} opens the gateway to access two (out of three) remaining unknown parameters in the neutrino Standard Model: the neutrino mass hierarchy and the leptonic CP phase δ_{CP}. [b]

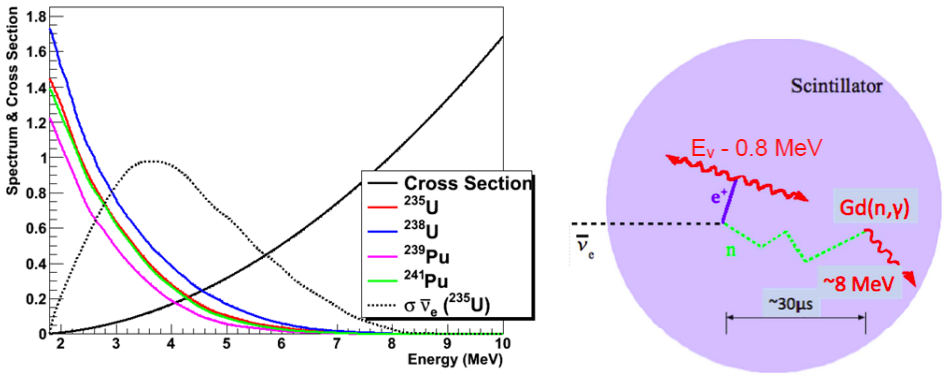

Fig. 1. (Left) $\bar{\nu}_e$ energy spectra (four curves with negative slopes) for ^{235}U, ^{238}U, ^{239}Pu, and ^{241}Pu are shown. The curve with positive slope represents the cross section of the inverse beta decay (IBD) process. The convoluted IBD spectrum, seen in experiments, is shown as the dotted line. (Right) The detecting principle of IBD is shown.

Reactor is essentially a pure electron antineutrino $\bar{\nu}_e$ source with an average of six $\bar{\nu}_e$ produced per fission along the β-decay chain of fission products. [c] For a 1 GW reactor thermal power, about 2×10^{20} $\bar{\nu}_e$ are emitted every second isotropically. Inside the reactor core, the fission process is maintained by neutrons produced through the fission of ^{235}U nucleus. The condition is adjusted so that only one neutron out of the few generated by the ^{235}U fission can induce a new fission. Meanwhile, a portion of the neutrons are captured by the ^{238}U producing new fissile isotopes: ^{239}Pu and ^{241}Pu. These four isotopes are main sources of $\bar{\nu}_e$. The $\bar{\nu}_e$ energy spectra are shown in the left panel of Fig. 1.

As shown in the right panel of Fig. 1, reactor $\bar{\nu}_e$ is detected through the inverse beta decay (IBD) reaction with free protons: $\bar{\nu}_e + p \rightarrow e^+ + n$. An IBD event is a pair of coincident signals consisting i) a prompt signal induced by the positron ionization and annihilation inside the detector (such as a liquid scintillator LS detector) and ii) a delay signal produced by the neutron capture on proton or nucleus (such as Gd). In particular, the neutron capture on Gd would release multiple gammas with a total energy $\sim$8 MeV. With 0.1% Gd doped LS, the mean time between the

[b] The other unknown parameter is the mass of the lightest neutrino.
[c] There is a small component of the electron neutrino ν_e with energy $\sim$0.1 MeV from the neutron activation of shielding materials.

prompt and the delay signal is about 30 μs. Due to the time-correlation nature, IBD can be easily distinguished from radioactive backgrounds which mostly consist of only a single signal. Furthermore, the energy of the prompt signal is directly linked to the neutrino energy: $E_\nu \approx E_{prompt} + 0.78$ MeV. This is in particular an attractive feature for measurements of neutrino oscillations that require knowledge of the neutrino energy. The left panel of Fig. 1 shows the total cross section of the IBD process and the convoluted energy spectrum in reactor experiments.

The current-generation reactor neutrino experiments including Daya Bay, Double Chooz, and RENO are designed to measure the third neutrino mixing angle θ_{13} in the neutrino mixing (commonly referred to as the Pontecorvo-Maki-Nakagawa-Sakata or PMNS in short [5,6,7]) matrix. The survival probability of $\bar{\nu}_e$ with energy E_ν at a distance L is written as:

$$P_{\bar{\nu}_e \to \bar{\nu}_e} = 1 - \sin^2 2\theta_{13} \cdot \sin^2 \left(\Delta m^2_{ee} \cdot \frac{L}{E_\nu} \right) - \cos^4 \theta_{13} \cdot \sin^2 2\theta_{12} \cdot \sin^2 \left(\Delta m^2_{21} \cdot \frac{L}{E_\nu} \right). \quad (1)$$

Here, $\Delta m^2_{ij} := m^2_i - m^2_j$ are neutrino mass-squared differences. From Ref. [8], we have $\Delta m^2_{21} \approx 7.6 \times 10^{-5}$ eV^2 and $\Delta m^2_{ee} \approx 2.4 \times 10^{-3}$ eV^2 that is a combination of Δm^2_{32} and Δm^2_{31} [9]. $\theta_{12} \sim 32^\circ$ [8] is the second neutrino mixing angle. From Eq. (1), it is easily seen that the $\bar{\nu}_e$ disappearance is a very clean channel to access θ_{13}. Unlike the $\nu_\mu \to \nu_e$ appearance channel, the disappearance channel is not sensitive to the mass hierarchy (sign of Δm^2_{32}) through the matter effect and is immune to the unknown CP phase δ_{CP} in the PMNS matrix.

The first attempt to measure θ_{13} is by CHOOZ [10,11] and Palo Verde [12] experiments in late 1990s and early 2000s. No oscillations were observed and an upper limit of $\sin^2 2\theta_{13} < 0.12$ was set at 90% C.L. by Chooz. In 2011, there were several hints suggesting a non-zero θ_{13}. The first one is from the tension [13] between the KamLAND $\bar{\nu}_e$ disappearance measurement and the solar measurements (e.g. ratio of ν_e to the neutral current interactions from SNO). Subsequently, MINOS [14] and T2K [15] reported their searches of ν_μ to ν_e oscillation that is also sensitive to θ_{13}. In particular, T2K [15] disfavored the $\theta_{13} = 0$ hypothesis at 2.5σ. In early 2012, Double Chooz [16] reported that the $\theta_{13} = 0$ hypothesis was disfavored at 1.6σ with only the far detector. A $>5\sigma$ discovery of non-zero θ_{13} was finally made by Daya Bay in March 2012 [4]. One month later, RENO confirmed the Daya Bay discovery with a 4.9σ significance [17]. Non-zero θ_{13} was firmly established. Fig. 2 shows the current-global status of $\sin^2 2\theta_{13}$ measurements compiled with the latest results from each experiment.

In the following, we review current-generation reactor experiments and present an outlook of future reactor experiments. As shown in Eq. (1), a non-zero θ_{13} will lead to $\bar{\nu}_e$ disappearance at $\sim$2 km corresponding to the oscillation length of the atmospheric mass-squared difference at E_ν =4 MeV (the peak of the reactor IBD energy spectrum). In practice, the search for such a deficit with a single detector is limited by the theoretical uncertainty of the antineutrino flux, which was considered to be larger than the speculated deficit when the current-generation experiments

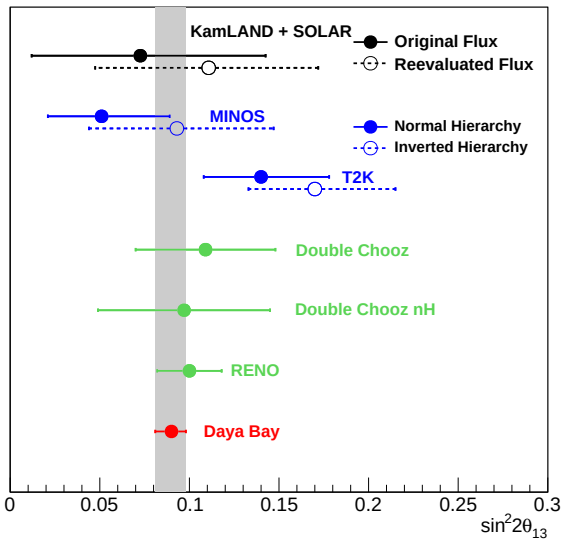

Fig. 2. Global status of $\sin^2 2\theta_{13}$ including KamLAND+SOLAR [13], MINOS [18], T2K [19], Double Chooz [20], RENO [21], and Daya Bay [22].

were designed. In order to suppress this uncertainty, the current generation experiments adopt the ratio strategy [23], in which identical detectors were deployed close to (near detectors at 0.3-0.5 km) and further away from (far detectors at 1-2 km) reactor cores. This dual-detector configuration is essential to achieve high precision measurements of $\sin^2 2\theta_{13}$.

The large size of θ_{13} has generated new opportunities which include the resolution of the neutrino mass hierarchy at medium-baseline reactor oscillation (MBRO) experiments. We will provide a brief review of MBRO principle and the JUNO experiment. Furthermore, a new evaluation of the reactor antineutrino flux revealed a discrepancy of about 5.7% between the calculation and very short baseline (< 100 m) measurements [24]. This deficit is usually referred to as the "reactor anomaly". An updated analysis, including kilometer-scale reactor experiments and improved treatment of correlations among experiments suggested a smaller discrepancy of 4.1% [25]. Recently, authors of Ref. [26] suggested that the uncertainty of reactor neutrino flux should be larger than 5%. To provide a definite answer, a new generation of very short-baseline (VSBL) reactor neutrino experiments have been proposed to address the "reactor anomaly". We will briefly review one U.S. effort, PROSPECT.

2. Daya Bay Reactor Neutrino Experiment

2.1. *Design of the experiment*

Daya Bay Reactor Neutrino Experiment is located on the campus of the Daya Bay nuclear reactor power plant in South China. As shown in the left panel of Fig. 3, the plant hosts six reactor cores whose locations are grouped into two clusters: the Daya Bay cluster that includes Daya Bay I and II cores and the Lingao cluster that includes Lingao I through IV cores. The total thermal power is about 17.4 GW. To monitor the antineutrino fluxes from these two clusters, Daya Bay has designed two near underground sites, the Daya Bay site (363 m from Daya Bay cores) and the Lingao site (∼500 m from Lingao cores). Each near underground site hosts two antineutrino detectors (ADs). The far site is located at a position that maximizes the sensitivity to θ_{13}, considering the overburden and geological conditions for the construction of an underground lab. The average baseline is about ~ 1.7 km. The near-far arrangement of the experiment guarantees that the reactor antineutrino flux uncertainty is largely canceled. The far site hosts four ADs which pair with the four ADs of the two near sites, providing a maximal cancellation of detector effects. The effective vertical overburdens are 250, 265, and 860 water-equivalent meters for EH1, EH2, and EH3, respectively.

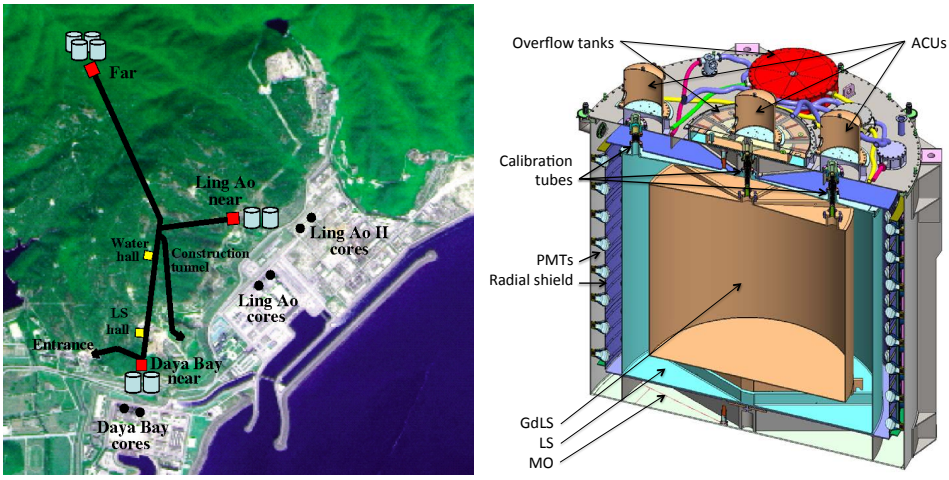

Fig. 3. Left panel shows the layout and the map of the Daya Bay experiment and the hosting Daya Bay plant campus. Right panel shows the structure of the Daya Bay antineutrino detector (AD). The Daya Bay ADs are equipped with three automated calibration units (ACUs), two for the Gd-LS volume and one for the LS volume.

Right panel of Fig. 3 shows the schematic view of the antineutrino detector (AD) [27]. Daya Bay adopts a three-zone cylindrical shaped design, with inner, middle, and outer layer containing 20 t Gd-doped (0.1% in weight) LAB-based liquid scintillator (GdLS), 22 t liquid scintillator (LS), and 40 t mineral oil, respec-

tively. 192 8-inch PMTs are installed on each AD. The photo-cathode coverage is about 8%, which is further enhanced by the top and bottom optical reflectors to about 12%. Three automated calibration units (ACUs) [28] are equipped. Each ACU contains four sources: i) a LED for the PMT gain/timing calibration, ii) a ^{68}Ge source for the IBD threshold calibration, iii) a ^{60}Co source for the determination of the overall energy scale, and iv) a ^{241}Am-^{13}C neutron source to understand neutron captures on Gd and to determine the H to Gd neutron capture ratio in the target (GdLS) region.

ADs are placed inside high purity water to reduce radioactive backgrounds from the environment. Each water pool is divided into two optically separated regions: the inner water pool (IWS) and the outer water pool (OWS). With PMTs installed, each region of water pool also operates as an independent water Cerenkov detector. The detection efficiencies for cosmic muons are measured to be 99.7% and 97% for the IWS and OWS [29], respectively. A layer of resistive plate chamber (RPC) is further installed above each water pool as an additional muon tagging detector.

2.2. *Signal and Backgrounds*

The IBD events in Daya Bay are selected with the following cuts [4,22]: i) the energy of the prompt signal is between 0.7 and 12 MeV, ii) the energy of the delay signal is between 6 and 12 MeV, and iii) the time difference between the prompt and the delay signal is between 1 and 200 μs. In addition, a multiplicity cut is applied to remove energy ambiguities in the prompt signal. The overall selection efficiency is about 80%. In order to suppress cosmogenic backgrounds, three types of muon vetos are applied to the delay signal: i) the water pool muon: from 2 μs before to 600 μs after the water pool signal, ii) the AD shower muon ($> 3 \times 10^5$ photoelectrons): from 2 μs before to 0.4 s after the AD shower, and iii) the AD non-shower muon (>20 MeV): from 2 μs before to 1.4 ms after the AD signal.

There are in total five backgrounds [4,22]. The first one is the accidental background, which consists two uncorrelated single signals, and can be calculated with negligible systematic uncertainties with the measured rate of single signal. It is about 1.7% and 4.6% of IBDs at near and far sites, respectively. The second one is the correlated background induced by the Am-C neutron source inside ACU. The energetic neutron could go through an inelastic scattering with an Fe nuclei emitting a gamma and then followed by an Fe capture emitting another gamma. The correlated background occurs when both gammas enter the AD. The rate of this background was estimated by the simulation and further validated by a special run with a strong Am-C source. It is about 0.03% and 0.3% of IBDs at near and far site, respectively. The relative uncertainty is about 30%. The third background is ^{9}Li and ^{8}He generated by cosmic muons. They are both long-lived isotopes which can not be excluded by muon vetos. They would firstly go through beta-decay process (prompt). The daughter nucleus could emit a neutron (delay). The rates can be directly measured by tagging muons. They are about 0.35% and 0.2% of IBDs

at near and far site, respectively. The uncertainties are about 30-50%. The fourth background is the fast neutrons produced by cosmic muons. The fast neutrons could go through an elastic scattering with proton (prompt) and followed by a capture (delay). They can also be directly measured by tagging the muon. It is about 0.13% and 0.1% for the near and far sites, respectively. The uncertainty is about 30%. The last background (α-N) is induced by internal radioactive backgrounds and is below 0.1%. Besides backgrounds, the detector related uncertainties entering into the oscillation analysis are dominated by the 0.12% from the 6 MeV delay energy cut and $\sim$0.1% from the H to Gd neutron capture ratio. The reactor related uncertainties, suppressed by near/far ratios, are $\sim$0.04%.

2.3. *Detector Energy Calibration*

Reactor IBD spectrum covers the antineutrino energy range from from 1.8 MeV to $\sim$8 MeV. The analysis of the spectral distortion between the near and far detectors can provide additional information on $\sin^2 2\theta_{13}$ as well as new information on Δm^2_{ee}. In this analysis, understanding the absolute energy response of the prompt positron signal is crucial. The LS energy response in Daya Bay is illustrated in the following. First, a positron with a kinetic energy E_{true} would deposit E_{dep} into the LS through the ionization and the annihilation processes. Second, some of the deposited energy will convert to scintillation light and Cerenkov radiation. Due to the quenching process of the LS, the conversion between E_{dep} and scintillation light is not linear. In addition, Cerenkov radiation emerges only when the particle is above the Cerenkov threshold of the LS. Total light collected by PMTs including both scintillation and Cerenkov lights is referred to as the visible energy E_{vis}. Finally, the readout electronics will convert E_{vis} into the reconstructed energy E_{rec} used in the oscillation analysis. The conversion between E_{true} and E_{vis} is referred to as the scintillator nonlinearity. The conversion between E_{vis} and E_{rec} is referred to as the electronics nonlinearity.

In Daya Bay, the scintillator energy model is based on the LS response to electron. The response to gamma is connected to that to electron through a GEANT4 simulation. [d] The detector response to the ionization energy loss of positron is assumed to be the same as that to electron. There are two additional 0.511 MeV gammas from the positron annihilation. Two approaches are used to parametrize the LS response to electron: i) Birks law for scintillation plus Cerenkov contributions and ii) direct parametrization inspired by i). The functional form of the electronics nonlinearity is inspired by the Monte Carlo simulation of the electronics.

The energy model is constrained by the calibration with gamma sources and the well-known ^{12}B beta decay continuous spectrum. The gamma sources include i) regularly deployed radioactive calibration sources: ^{68}Ge, ^{60}Co, and ^{241}Am-^{13}C, ii)

[d]Gammas deposit energy in LS via electrons/positrons produced through Compton scatterings and pair productions.

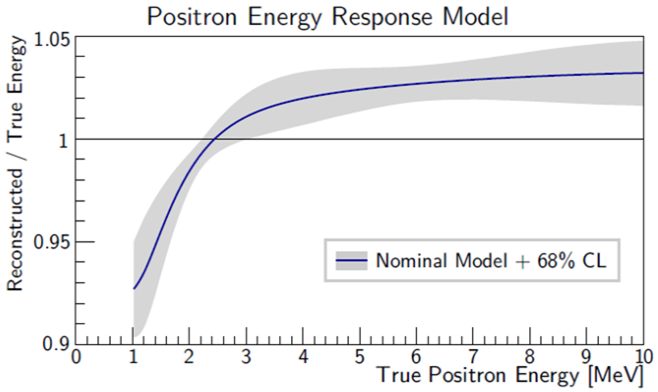

Fig. 4. The Daya Bay positron energy model taken from Ref. [22].

additional radioactive sources deployed during a special calibration period: ^{137}Cs, ^{54}Mn, ^{40}K, ^{241}Am-^{9}Be, and Pu-^{13}C, and iii) singles during regular physics data taking: ^{40}K, ^{208}Tl, and n-H capture. The ^{12}B that are produced by the muon spallation inside the scintillator are selected by tagging the muon signal. In addition, the model is further checked with α peaks from ^{210}Po, ^{219}Rn, ^{212}Po, ^{214}Po, and ^{215}Po and continuous beta-decay spectra from ^{212}Bi, ^{214}Bi, and ^{208}Tl. Several models are independently developed by different analysis teams, and the final positron energy model is conservatively taken as linear combinations of five energy models. Fig. 4 shows the Daya Bay positron energy model and its uncertainty band [22].

2.4. $\sin^2 2\theta_{13}$ and Δm^2_{ee}

The oscillation analysis is based on the standard χ^2 method with Poisson statistics. The variations in systematics are included as penalty terms in the χ^2. The rate-only analysis [4] of full 6-AD data (∼215 days of data taking) yields $\sin^2 2\theta_{13} = 0.089 \pm 0.009$ with χ^2/NDF=0.48/4. In this analysis, the constraint of Δm^2_{ee} is added according to the MINOS measured $\Delta m^2_{\mu\mu} = 2.41^{+0.09}_{-0.10} \times 10^{-3}$ eV^2 [30]. In the Daya Bay rate+shape analysis, uncertainties in the reactor flux predictions are based on Ref. [31,32,33,34,35,36]. The constraint is implemented as a covariance matrix in the penalty terms. The rate+shape analysis yields $\sin^2 2\theta_{13} = 0.090^{+0.008}_{-0.009}$ and $\Delta m^2_{ee} = 2.59^{+0.19}_{-0.20} \times 10^{-3}$ eV^2 with χ^2/NDF=162.7/153 [22]. The Δm^2_{ee} result corresponds to $\Delta m^2_{32} = 2.54^{+0.19}_{-0.20} \times 10^{-3}$ eV^2 assuming the normal mass hierarchy or $\Delta m^2_{32} = -2.64^{+0.20}_{-0.19} \times 10^{-3}$ eV^2 assuming the inverted mass hierarchy. These results are consistent with the $\Delta m^2_{\mu\mu}$ measured in MINOS ($\Delta m^2_{32} = 2.37^{+0.09}_{-0.09} \times 10^{-3}$ eV^2 assuming the normal mass hierarchy or $\Delta m^2_{32} = -2.41^{+0.11}_{-0.09} \times 10^{-3}$ eV^2 assuming the inverted mass hierarchy) [30]. Fig. 5 shows the best-fit IBD spectra in all three experimental halls. In addition, we show the electron antineutrino survival probability vs. the effective propagation distance L_{eff} over E_ν.

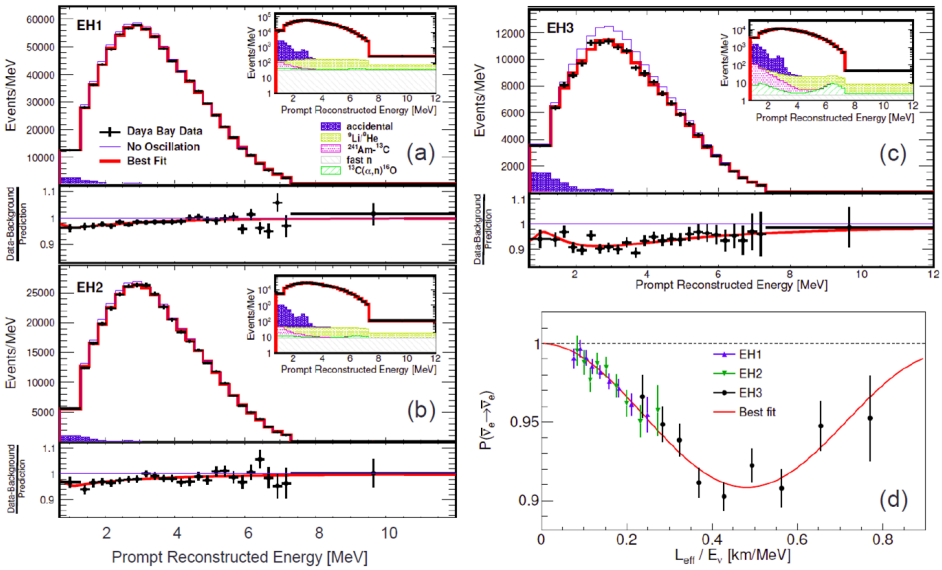

Fig. 5. 6-AD data and best-fit spectra in three experimental halls are shown as a), b), and c). The electron antineutrino survival probability vs. the effective propagation distance L_{eff} over the antineutrino energy E_ν is shown in d). An effective detector-reactor distance L_{eff} is calculated for each experimental hall by treating the multi-core oscillated flux as it is from a single reactor core. Plots are taken from Ref. [22].

2.5. *Outlook*

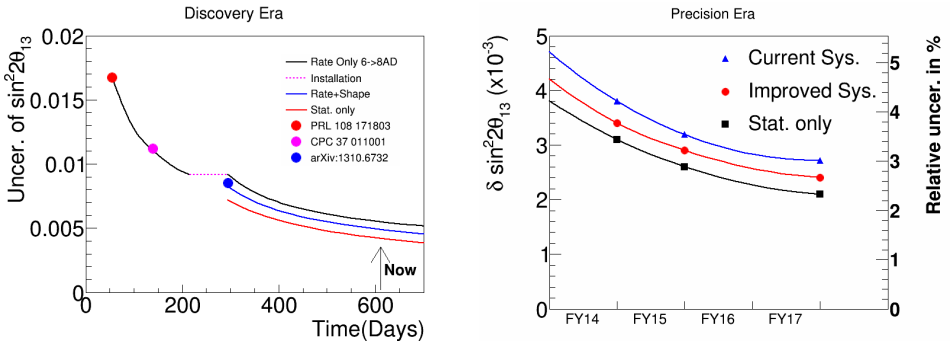

Fig. 6. (Left) Uncertainty on the Daya Bay measurement of $\sin^2 2\theta_{13}$ over time under different assumptions. (Right) Uncertainty on the Daya Bay measurement of $\sin^2 2\theta_{13}$ in the precision era (FY14-FY17) under different assumptions. Plots are taken from Ref. [37].

Daya Bay is entering the precision phase with data taking through 2017 [37]. As shown in Fig. 6, the $\sin^2 2\theta_{13}$ will be measured to better than 3% (an absolute uncertainty of 0.003). It will stand as the world's most precise measurement for

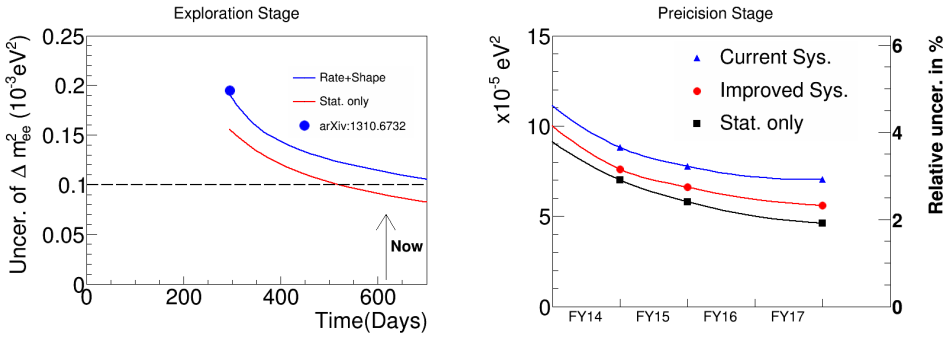

Fig. 7. (Left) The expected Daya Bay uncertainty on Δm^2_{ee} with existing systematic uncertainties and the statistical-only uncertainty. The horizontal dash line is the current MINOS uncertainty in $\Delta m^2_{\mu\mu}$. (Right) The evolution of the Daya Bay's uncertainty on Δm^2_{ee} is shown for a few different scenarios in the precision era. Plots are taken from Ref. [37].

the foreseeable future. The precision measurement of $\sin^2 2\theta_{13}$ will also improve the measurement of other mixing parameters by accelerator experiments. Furthermore, the comparison of the precision measurement of $\sin^2 2\theta_{13}$ in reactor experiments and that from accelerator experiments (such as LBNE [38]) will be one of the most stringent unitarity tests of the PMNS neutrino mixing matrix [39]. This is a crucial test of the standard 3-flavor neutrino framework in analogy to the unitarity test of the quark-mixing (CKM) matrix.

As shown in Fig. 7, Daya Bay will reach a precision of Δm^2_{ee} to about 2.5%, which will be competitive with that of $\Delta m^2_{\mu\mu}$ currently set by MINOS. This will be another stringent test to the 3-flavor neutrino framework. In addition, the comparison of Δm^2_{ee} and $\Delta m^2_{\mu\mu}$ will provide additional information regarding to the neutrino mass hierarchy.

Daya Bay will have the largest sample of reactor IBD events with more than one million interactions. Such a large sample of IBDs will provide excellent opportunities to study the reactor antineutrino spectrum as well as a precision flux measurement at a distance of ∼360 m. In addition, with the unique three sites configuration (e.g. three baselines), Daya Bay allows a competitive search for a sterile neutrino in the mass-squared splitting range of 0.001-0.2 eV^2 with excellent sensitivities.

3. RENO

RENO is another current-generation short-baseline reactor neutrino experiment aiming at measuring the value of $\sin^2\theta_{13}$ and it has confirmed the Daya Bay discovery of non-zero θ_{13} with a near 5-σ confidence level. The experiment is built near the Yonggwang nuclear power plant in South Korea. The total thermal power of the six reactor cores is about 16.4 GW. The baseline distribution of RENO is shown in Fig. 8. With a symmetric core configuration, RENO has one near site and one far site to suppress the reactor antineutrino flux uncertainty. The distance between

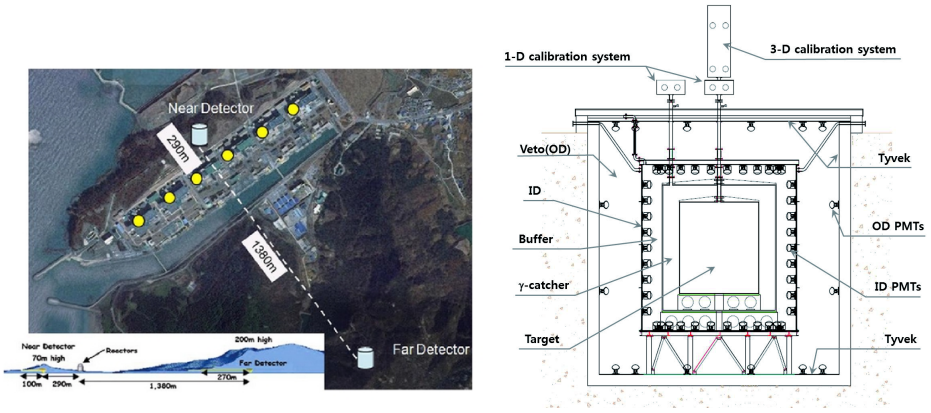

Fig. 8. The left panel shows the Yonggwang nuclear reactor complex. The six reactors are equally spaced on one line. RENO near site is located ∼290 m away from the reactor complex center and the far site is ∼1,380 m away. The overburden is 70 m rock (185 meter water equivalent or mwe) at the near site and 200 m (530 mwe) at the far site. The right panel shows RENO's detector system. A 3-D calibration system is installed in the GDLS. The gamma catch region is equipped with a 1-D calibration system which moves calibration sources along the vertical direction.

RENO's near site and the geometrical center of reactor cores is ∼290 m. For the far site, the distance is ∼1,380 m. The arrangement of the RENO detector system has taken a similar approach as the Daya Bay one: a three-zone LS antineutrino detector is nested in a muon veto system. The RENO LS is also LAB-based. The target zone contains 16.1 t 0.1% Gd-doped LS.

RENO had collected ∼800 live days of data by the end of 2013 and its statistical uncertainty has surpassed the systematic one. The latest result based on the rate analysis of RENO is $\sin^2 2\theta_{13} = 0.100 \pm 0.010$ (stat.) ± 0.015 (sys.) [21].

4. Double Chooz

Double Chooz experiment is built upon the previous generation Chooz experiment that set the best $\sin^2 2\theta_{13}$ upper limit previously. The Double Chooz design expands the Chooz one by adding a near site which monitors the antineutrino flux from the two nuclear reactors at a distance of ∼410 m. The near site's overburden is 115 mwe. Double Chooz's far site is the original Chooz detector site whose baseline is 1,067 m and an overburden of 300 mwe. The total thermal power of the two Double Chooz reactors is 8.7 GW. Figure 9 shows the Double Chooz map and the detector design. The Double Chooz detector, like all current-generation reactor antineutrino detectors, adapts a three-zone design with the inner-most Gd-doped LS region as the target. Double Chooz chooses PXE-based LS. The Gd doping is about 1 g/l. Its target mass is 10 t. Light from the target and the γ-catcher regions is monitored by 390 low-background 10-inch PMTs.

Due to the delay in the civil construction, Double Chooz has so far only collected far-site data. To constrain the reactor antineutrino flux uncertainty, Dou-

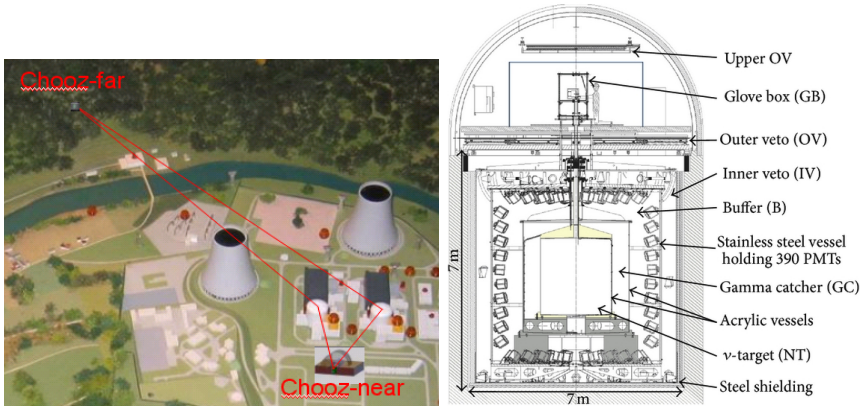

Fig. 9. (Left) The two nuclear reactors and the two detector locations of Double Chooz are shown. Double Chooz's near site is located ∼410 m away and the far site is the original Chooz site which is ∼1,067 m away. The overburden is 115 mwe and 300 mwe at the near and far site, respectively. (Right) The Double Chooz detector system.

ble Chooz has used Bugey-4 measurement [40] as the flux normalization. The Double Chooz analysis based on the neutron capture on Gd data gives $\sin^2 2\theta_{13} = 0.109 \pm 0.030$ (stat.) ± 0.025 (sys.), which has considered the prompt energy spectrum [41]. Double Chooz has also carried out an independent θ_{13} analysis using the neutron capture on H data [20]. The H-capture measurement, $\sin^2 2\theta_{13} = 0.097 \pm 0.034$ (stat.) ± 0.034 (sys.), is consistent with the Gd result. One advantage of Double Chooz is its fewer number of reactors which can create a unique reactor off data-taking condition. The direct background measurement during the 7.53 days of reactor-off period has enabled a background-independent θ_{13} analysis [42]. Combining the data of neutron captures on both Gd and H, Double Chooz measures $\sin^2 2\theta_{13} = 0.102 \pm 0.028$ (stat.) ± 0.033 (sys.). The Double Chooz near detector is expected to start data taking in early 2014.

5. Future Reactor Neutrino Experiments

The current-generation reactor experiments will perform the ultimate measurement of $\bar{\nu}_e$ disappearance at a short baseline ($\sim$ 2 km). Future reactor-based experiments will focus on the very short baseline (VSBL) and the medium baseline for different purposes. As examples, we pick one from each category, PROSPECT in the U.S. from VSBL experiments and JUNO in China from medium-baseline experiments. The PROSPECT experiment aims at resolving the reactor anomaly [24] at baselines $\sim$ 4-20 m. The JUNO experiment's major motivations includes the determination of the neutrino mass hierarchy and precision measurements of neutrino mixing parameters at baselines of ∼53 km.

5.1. *PROSPECT*

PROSPECT (a Precision Reactor Oscillation and Spectrum Experiment at Very Short Baselines) is a multi-phased, multi-purposed, very short-baseline, research-reactor based, neutrino experiment proposed in the U.S. [43] The collaboration is currently looking at three potential research reactor sites, the Advanced Test Reactor (ATR) at the Idaho National Laboratory (INL), the High Flux Isotope Reactor (HFIR) at Oak Ridge National Laboratory (ORNL), and the National Bureau of Standards Reactors (NBSR) at National Institute of Standards and Technology (NIST). The research reactor sites generally allows baselines as short as a few meters, which are the most interested region for the sterile neutrino search hinted by the reactor anomaly [24]. To enhance the sensitivity to an extra mass eigenstate whose mass-squared splitting with the active states is at $\sim$1 eV^2, PROSPECT collaboration adopts a segmented detector design to provide essential resolutions in L/E. PROSPECT also has a unique phased approach. In its first phase, a near detector within 10 m from the reactor core will be installed and PROSPECT will cover L/E in the range of 0.5-2.5 m/MeV. In its second phase, PROSPECT will install a far detector with a baseline of 10-20 m, which will extend the L/E coverages to 6 m/MeV. With these L/E coverages, PROSPECT will be able to exclude most of the parameter space allowed by the reactor anomaly with high confidence levels.

Besides its high quality data providing a definite test on the reactor anomaly, PROSPECT data also has great potential in constraining reactor antineutrino flux for other reactor neutrino experiments and for the nuclear non-proliferation industry. All three candidate research reactors of PROSPECT use highly-enriched uranium (HEU) whose antineutrinos are almost exclusively from ^{235}U fissions. The ^{235}U antineutrino flux is the most precisely predicted one based on the ILL beta spectrometer measurement [31,32]. Therefore, PROSPECT will be able to provide an valuable benchmark to the reactor antineutrino flux prediction and the reactor core simulation. Combined with existing flux measurements at commercial reactors, PROSPECT data can also be used to test the flux calculations other than ^{235}U. Improved knowledge in the reactor antineutrino flux prediction is going to be highly valuable to future reactor based neutrino experiments. The high precision measurement of the reactor antineutrino spectrum at a near-surface operation will also naturally benefit the development of reactor safeguards.

5.2. *Jiangmen Underground Neutrino Observatory*

JUNO will be built in the Jiangmen City, Guangdong Province, China [44,45,46]. The central piece of this experiment is a 20 kt liquid scintillator detector. This detector will observe $\bar{\nu}_e$ from two reactor complexes: Taishan and Yangjiang. The Taishan reactor complex contains six reactor cores with a total thermal power of 17.4 GW. The Yangjiang reactor complex has two reactor cores with a total thermal power of 9.2 GW. There are two additional reactor cores (9.2 GW) planned at the Yangjiang

site. The average baseline of JUNO is ∼52.5 km with a RMS (root mean square) of 0.25 km. The construction and the data taking are expected to start in 2015 and 2020, respectively.

Through the measurement of $\bar{\nu}_e$ disappearance at ∼53 km, JUNO's major physics goals are: i) the first experiment to simultaneously observe neutrino oscillations from both the atmospheric and the solar neutrino mass-squared splittings (see the left panel of Fig. 10), ii) the first experiment to observe more than two oscillation cycles of the atmospheric mass-squared splitting (see the left panel of Fig. 10), iii) determination of the neutrino mass hierarchy, whether Δm^2_{32} is larger or smaller than zero, through the measurement of the spectral distortion, and iv) precision measurements of $\sin^2 2\theta_{21}$, Δm^2_{32}, and Δm^2_{21} to better than 1%. We should note that the precision measurement of Δm^2_{32} requires the knowledge of the neutrino mass hierarchy. Besides these, the 20 kt detector offers a rich physics program of the proton decay, geoneutrinos, supernova neutrinos, and many exotic neutrino physics topics.

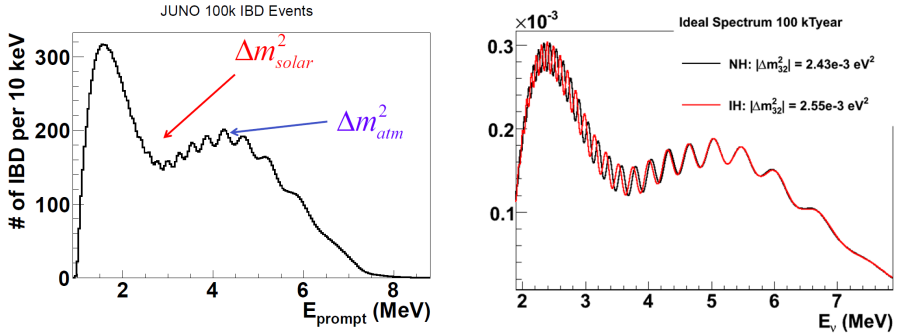

Fig. 10. (Left) The expected nominal prompt energy spectrum of JUNO. A total of 100k IBD events, which corresponds to six years of data taking with a 20 kt detector and 36 GW_{th} reactor power, is assumed. The big dip around 3 MeV corresponds to the solar oscillation (Δm^2_{21}). The small wiggles from 2 to 8 MeV correspond to the atmospheric oscillation (Δm^2_{ee}). A $3\%/\sqrt{E\ (MeV)}$ energy resolution is assumed. (Right) The ideal spectral distortion at JUNO (arbitrary scale in the vertical axis) for both normal and inverted hierarchies with a perfect energy resolution. Plots are taken from Ref. [47].

The neutrino mass hierarchy (MH) is likely to be the next determined fundamental parameter in the neutrino Standard Model. In combination with searches for the neutrinoless double beta decay, the determination of MH will provide crucial information regarding the nature of neutrinos (whether they are Dirac or Majorana fermions). The non-zero θ_{13} established by the current-generation reactor experiments opened the path to determine the MH in a medium baseline (∼55 km) reactor experiment [49,50,51,52,53,54,55,48]. One simple way to understand the principle of MH determination is through the effective mass-squared splitting Δm^2_{ee}. At 55 km baseline, the Δm^2_{ee} measured at low energy (∼3 MeV) will be different from

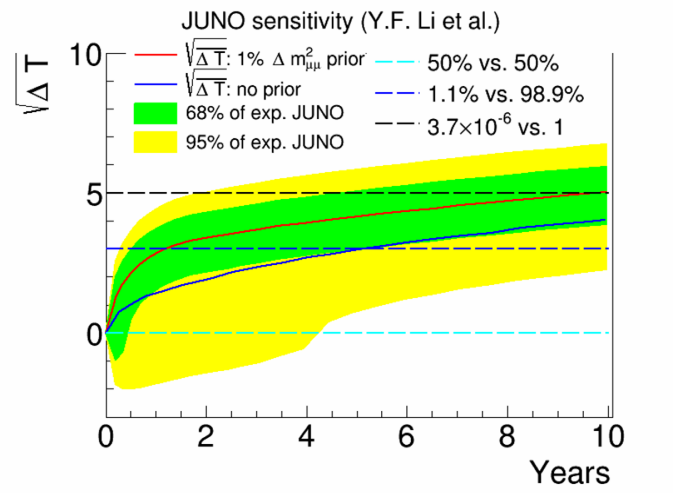

Fig. 11. JUNO's sensitivity evolution with respect to calendar years. [48]. A 20 kt detector at ∼ 53 km with a total of 36 GW_{th} reactor power was assumed. The energy resolution was assumed to be $3\%/\sqrt{E\ (MeV)}$. Plot is taken from Ref. [47].

that measured at high energy (∼6 MeV). For the normal MH, Δm^2_{ee} at low energy will be larger than that at high energy, and vice versa for IH. The difference in the spectral distortion (with a perfect energy resolution) for NH and IH is shown in the right panel of Fig. 10. In order to reach this goal, JUNO requires i) a better than $\sim 3\%/\sqrt{E(MeV)}$ energy resolution, ii) a high statistics IBD sample (>100k), iii) a <1% absolute energy scale uncertainty [53,56]. In addition, the site choice of JUNO was optimized taking into account the locations of reactor cores. Figure 11 shows the expected sensitivity of JUNO [48] with respect to the running time. The ΔT is a test statistics consisting likelihoods of normal and inverted MH for data x. The green and yellow bands represent the 68% and 95% expectations, respectively, taking into account the fluctuations in statistics and variations in systematics. The dotted lines correspond to the probability ratios of the normal vs. inverted MH in the Bayesian framework [57].

In addition to the determination of MH, JUNO will perform precision measurement of neutrino mixing, which is a powerful tool to test the standard 3-flavor neutrino framework (or νSM). The precision measurement of $\sin^2 2\theta_{12}$ will i) lay the foundation for a future sub-1% direct unitarity test of the PMNS matrix [58,39], ii) constrain the allowed region of the effective neutrino mass to which the decay width of neutrinoless double beta decay is proportional, and iii) test models of neutrino masses and mixing [59], such as $\theta_{12} = 35^\circ + \theta_{13}\cos\delta$, $\theta_{12} = 32^\circ + \theta_{13}\cos\delta$, and $\theta_{12} = 45 + \theta_{13}\cos\delta$. The precision measurement of Δm^2_{ee} (or Δm^2_{32}) will i) test an important sum rule $\Delta m^2_{13} + \Delta m^2_{21} + \Delta m^2_{32} = 0$ and ii) reveal additional information regarding the neutrino mass hierarchy, when combined with the precision $\Delta m^2_{\mu\mu}$ measurements from muon (anti)neutrino disappearance in accelerator exper-

iments. As shown in Ref. [60], the expected JUNO's precision of Δm^2_{21}, Δm^2_{32}, and $\sin^2 2\theta_{21}$ are 0.3%, 0.3%, and 0.6%, respectively. Such precision potential is further confirmed by studies made in Ref. [56].

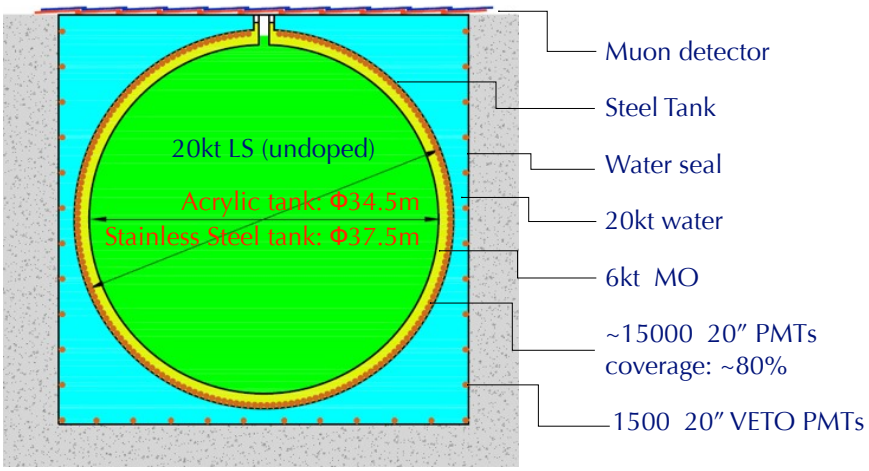

Fig. 12. One conceptual design of the JUNO detector. Unlike the current-generation short-baseline reactor antineutrino three-zone detectors, JUNO detector may adapt a two-zone design like the KamLAND one. And its target LS would be undoped due to the considerations of LS transparency and the unavoidable radioactive contamination in doping elements.

The central detector of JUNO will be a 20 kt underground liquid scintillator detector with a 1,850 m water equivalent overburden. Figure 12 shows one conceptual design of JUNO's 20 kt LS detector [61,62]. A spherical LS target volume is chosen i) to minimize the surface-to-volume ratio and PMT costs and ii) to minimize position dependent corrections to the reconstructed energy. The photo-cathode coverage is expected to reach ∼80%. Together with the high performance LS (high intrinsic photon yield with >14,000 photons per MeV, the superior optical attenuation length of 30 m or better) and the high quantum efficiency PMT, JUNO is aiming to achieve a better than $3\%/\sqrt{E\ (MeV)}$ energy resolution that is essential for MH determination.

6. Summary

There were many discoveries in neutrino oscillation physics in the last decade. With the current-generation reactor experiments, we now know the value of θ_{13} (Daya Bay: $\sin^2 2\theta_{13} = 0.090^{+0.008}_{-0.009}$). The large value of θ_{13} opens doors to access remaining unknowns in the νSM: the neutrino mass hierarchy and the leptoic CP phase δ_{CP}. In particular, the next generation (medium-baseline) reactor experiments aims to resolve the neutrino mass hierarchy. As we enter the precision era of neutrino physics, the current and future reactor experiments will bring us more exciting findings.

Acknowledgments

We would like to thank Zhizhong Xing, Dmitry Naumov, Karsten Heeger for helpful inputs. This work was supported in part by the National Science Foundation and the Department of Energy under contracts DE-AC02-98CH10886.

References

1. C.L. Cowan, F. Reines, F.B. Harrison, H.W. Kruse, and A.D. McGuire. Detection of the free neutrino: A Confirmation. *Science*, 124:103–104, 1956.
2. T. Araki et al. Measurement of neutrino oscillation with KamLAND: Evidence of spectral distortion. *Phys.Rev.Lett.*, 94:081801, 2005.
3. Q.R. Ahmad et al. Direct evidence for neutrino flavor transformation from neutral current interactions in the Sudbury Neutrino Observatory. *Phys.Rev.Lett.*, 89:011301, 2002.
4. F.P. An et al. Observation of electron-antineutrino disappearance at Daya Bay. *Phys.Rev.Lett.*, 108:171803, 2012.
5. B. Pontecorvo. Mesonium and anti-mesonium. *Sov.Phys.JETP*, 6:429, 1957.
6. B. Pontecorvo. Neutrino Experiments and the Problem of Conservation of Leptonic Charge. *Sov.Phys.JETP*, 26:984–988, 1968.
7. Ziro Maki, Masami Nakagawa, and Shoichi Sakata. Remarks on the unified model of elementary particles. *Prog.Theor.Phys.*, 28:870–880, 1962.
8. J. Beringer et al. Review of Particle Physics (RPP). *Phys.Rev.*, D86:010001, 2012.
9. H. Minakata, H. Nunokawa, Stephen J. Parke, and R. Zukanovich Funchal. Determining neutrino mass hierarchy by precision measurements in electron and muon neutrino disappearance experiments. *Phys.Rev.*, D74:053008, 2006.
10. M. Apollonio et al. Limits on neutrino oscillations from the CHOOZ experiment. *Phys.Lett.*, B466:415–430, 1999.
11. M. Apollonio et al. Search for neutrino oscillations on a long baseline at the CHOOZ nuclear power station. *Eur.Phys.J.*, C27:331–374, 2003.
12. F. Boehm, J. Busenitz, B. Cook, G. Gratta, H. Henrikson, et al. Final results from the Palo Verde neutrino oscillation experiment. *Phys.Rev.*, D64:112001, 2001.
13. G.L. Fogli, E. Lisi, A. Marrone, A. Palazzo, and A.M. Rotunno. Evidence of $\theta_{13} > 0$ from global neutrino data analysis. *Phys.Rev.*, D84:053007, 2011.
14. P. Adamson et al. Improved search for muon-neutrino to electron-neutrino oscillations in MINOS. *Phys.Rev.Lett.*, 107:181802, 2011.
15. K. Abe et al. Indication of Electron Neutrino Appearance from an Accelerator-produced Off-axis Muon Neutrino Beam. *Phys.Rev.Lett.*, 107:041801, 2011.
16. Y. Abe et al. Indication for the disappearance of reactor electron antineutrinos in the Double Chooz experiment. *Phys.Rev.Lett.*, 108:131801, 2012.
17. J.K. Ahn et al. Observation of Reactor Electron Antineutrino Disappearance in the RENO Experiment. *Phys.Rev.Lett.*, 108:191802, 2012.
18. Justin Evans. The MINOS experiment: results and prospects. *Adv.High Energy Phys.*, 2013:182537, 2013.
19. K. Abe et al. Observation of Electron Neutrino Appearance in a Muon Neutrino Beam. 2013.
20. Y. Abe et al. First Measurement of θ_{13} from Delayed Neutron Capture on Hydrogen in the Double Chooz Experiment. *Phys.Lett.*, B723:66–70, 2013.
21. S.-H. Seo. New Results from RENO. *ArXiv e-prints*, December 2013.
22. F.P. An et al. Spectral measurement of electron antineutrino oscillation amplitude

and frequency at Daya Bay. 2013.
23. L.A. Mikaelyan and V.V. Sinev. Neutrino oscillations at reactors: What next? *Phys.Atom.Nucl.*, 63:1002–1006, 2000.
24. G. Mention, M. Fechner, Th. Lasserre, Th.A. Mueller, D. Lhuillier, et al. The Reactor Antineutrino Anomaly. *Phys.Rev.*, D83:073006, 2011.
25. C. Zhang, X. Qian, and P. Vogel. Reactor Antineutrino Anomaly with known θ_{13}. *Phys.Rev.*, D87(7):073018, 2013.
26. A.C. Hayes, J.L. Friar, G.T. Garvey, and Guy Jonkmans. Reanalysis of the Reactor Neutrino Anomaly. 2013.
27. H.R. Band, R. Carr, X.C. Chen, X.H. Chen, J.J. Cherwinka, et al. Assembly and Installation of the Daya Bay Antineutrino Detectors. *JINST*, 8:T11006, 2013.
28. J. Liu, B. Cai, R. Carr, D.A. Dwyer, W.Q. Gu, et al. Automated Calibration System for a High-Precision Measurement of Neutrino Mixing Angle θ_{13} with the Daya Bay Antineutrino Detectors. 2013.
29. F.P. An et al. A side-by-side comparison of Daya Bay antineutrino detectors. *Nucl.Instrum.Meth.*, A685:78–97, 2012.
30. P. Adamson et al. Measurement of Neutrino and Antineutrino Oscillations Using Beam and Atmospheric Data in MINOS. *Phys.Rev.Lett.*, 110:251801, 2013.
31. F. Von Feilitzsch, A.A. Hahn, and K. Schreckenbach. EXPERIMENTAL BETA SPECTRA FROM PU-239 AND U-235 THERMAL NEUTRON FISSION PRODUCTS AND THEIR CORRELATED ANTI-NEUTRINOS SPECTRA. *Phys.Lett.*, B118:162–166, 1982.
32. K. Schreckenbach, G. Colvin, W. Gelletly, and F. Von Feilitzsch. DETERMINATION OF THE ANTI-NEUTRINO SPECTRUM FROM U-235 THERMAL NEUTRON FISSION PRODUCTS UP TO 9.5-MEV. *Phys.Lett.*, B160:325–330, 1985.
33. A.A. Hahn, K. Schreckenbach, G. Colvin, B. Krusche, W. Gelletly, et al. Anti-neutrino Spectra From ^{241}Pu and ^{239}Pu Thermal Neutron Fission Products. *Phys.Lett.*, B218:365–368, 1989.
34. Patrick Huber. On the determination of anti-neutrino spectra from nuclear reactors. *Phys.Rev.*, C84:024617, 2011.
35. P. Vogel, G.K. Schenter, F.M. Mann, and R.E. Schenter. Reactor Anti-neutrino Spectra and Their Application to Anti-neutrino Induced Reactions. 2. *Phys.Rev.*, C24:1543–1553, 1981.
36. Th.A. Mueller, D. Lhuillier, M. Fallot, A. Letourneau, S. Cormon, et al. Improved Predictions of Reactor Antineutrino Spectra. *Phys.Rev.*, C83:054615, 2011.
37. Daya Bay Collaboration. U.S. P5 contribution, `http://www.usparticlephysics.org/sites/default/files/webform/p5/DayaBay_RunPlan_0.pdf` (2013).
38. C. Adams et al. Scientific Opportunities with the Long-Baseline Neutrino Experiment. 2013.
39. X. Qian, C. Zhang, M. Diwan, and P. Vogel. Unitarity Tests of the Neutrino Mixing Matrix. 2013.
40. Y. Declais, H. de Kerret, B. Lefievre, M. Obolensky, A. Etenko, et al. Study of reactor anti-neutrino interaction with proton at Bugey nuclear power plant. *Phys.Lett.*, B338:383–389, 1994.
41. Y. Abe et al. Reactor electron antineutrino disappearance in the Double Chooz experiment. *Phys.Rev.*, D86:052008, 2012.
42. Y. Abe et al. Background-independent measurement of θ_{13} in Double Chooz. 2014.
43. J. Ashenfelter, A. B. Balantekin, H. Band, A. Bernstein, E. Blucher, N. S. Bowden, C. Bryan, J. C. Cherwinka, T. Classen, D. Dean, M. J. Dolinski, Y. Efremenko, A. Galindo-Uribarri, A. Glenn, M. Green, S. Hans, K. M. Heeger, R. Henning, L. Hu,

P. Huber, R. Johnson, C. Lane, T. J. Langford, J. G. Learned, B. R. Littlejohn, J. Maricic, B. McKeown, S. Morrell, H. P. Mumm, J. S. Nico, E. Romero, S. J. Thompson, W. Wang, B. White, R. E. Williams, T. Wise, M. Yeh, and N. Zaitseva. PROSPECT - A Precision Reactor Oscillation and Spectrum Experiment at Very Short Baselines. *ArXiv e-prints*, September 2013.

44. Yifang Wang. Daya Bay II: the next generation reactor neutrino experiment. In *NuFACT 2012*, Jul 2012.
45. Yifang Wang. Daya Bay II: current status and future plan. In *Daya Bay II First Meeting*, Jan 2013.
46. Yifang Wang. JUNO: current status and future plan. In *JUNO Meeting at IHEP, Beijing, China*, Jul 2013.
47. MBRO Collaboration. U.S. P5 contribution, `http://www.usparticlephysics.org/sites/default/files/webform/p5/US_JUNO_P5.pdf` (2014).
48. Yu-Feng Li, Jun Cao, Yifang Wang, and Liang Zhan. Unambiguous Determination of the Neutrino Mass Hierarchy Using Reactor Neutrinos. *Phys.Rev.*, D88:013008, 2013.
49. S.T. Petcov and M. Piai. The LMA MSW solution of the solar neutrino problem, inverted neutrino mass hierarchy and reactor neutrino experiments. *Phys.Lett.*, B533:94–106, 2002.
50. John Learned, Stephen T. Dye, Sandip Pakvasa, and Robert C. Svoboda. Determination of neutrino mass hierarchy and θ_{13} with a remote detector of reactor antineutrinos. *Phys.Rev.*, D78:071302, 2008.
51. Liang Zhan, Yifang Wang, Jun Cao, and Liangjian Wen. Determination of the Neutrino Mass Hierarchy at an Intermediate Baseline. *Phys.Rev.*, D78:111103, 2008.
52. Liang Zhan, Yifang Wang, Jun Cao, and Liangjian Wen. Experimental Requirements to Determine the Neutrino Mass Hierarchy Using Reactor Neutrinos. *Phys.Rev.*, D79:073007, 2009.
53. X. Qian, D.A. Dwyer, R.D. McKeown, P. Vogel, W. Wang, et al. Mass Hierarchy Resolution in Reactor Anti-neutrino Experiments: Parameter Degeneracies and Detector Energy Response. *PRD, 87,*, 033005, 2013.
54. Emilio Ciuffoli, Jarah Evslin, and Xinmin Zhang. The Neutrino Mass Hierarchy at Reactor Experiments now that theta13 is Large. *JHEP*, 1303:016, 2013.
55. Shao-Feng Ge, Kaoru Hagiwara, Naotoshi Okamura, and Yoshitaro Takaesu. Determination of mass hierarchy with medium baseline reactor neutrino experiments. *JHEP*, 1305:131, 2013.
56. A. B. Balantekin et al. Neutrino mass hierarchy determination and other physics potential of medium-baseline reactor neutrino oscillation experiments. 2013.
57. X. Qian, A. Tan, W. Wang, J.J. Ling, R.D. McKeown, et al. Statistical Evaluation of Experimental Determinations of Neutrino Mass Hierarchy. *Phys.Rev.*, D86:113011, 2012.
58. S. Antusch, C. Biggio, E. Fernandez-Martinez, M.B. Gavela, and J. Lopez-Pavon. Unitarity of the Leptonic Mixing Matrix. *JHEP*, 0610:084, 2006.
59. Stephen F. King, Alexander Merle, Stefano Morisi, Yusuke Shimizu, and Morimitsu Tanimoto. Neutrino Mass and Mixing: from Theory to Experiment. 2014.
60. Jun Cao. Daya bay-ii: A 60 km-baseline reactor experiment and beyond. In *International Symposium on Neutrino Physics and Beyond*, 2012.
61. Yue-Kun Heng. The central detector design and acrylic option. Jul 2013.
62. Yue-Kun Heng. The progress of the central detector. Oct 2013.